Stem Cell Reports
Article

ISSCR

OPEN ACCESS

4D imaging analysis of the aging mouse neural stem cell niche reveals a dramatic loss of progenitor cell dynamism regulated by the RHO-ROCK pathway

Xiuli Zhao,[1,3] Elizabeth S. Fisher,[1,3] Yue Wang,[1] Kristen Zuloaga,[2] Luke Manley,[1] and Sally Temple[1,*]
[1]Neural Stem Cell Institute, Rensselaer, NY 12144, USA
[2]Department of Neuroscience and Experimental Therapeutics, Albany Medical Center, Albany NY 12208, USA
[3]These authors contributed equally
*Correspondence: sallytemple@neuralsci.org
https://doi.org/10.1016/j.stemcr.2021.12.007

SUMMARY

In the adult ventricular-subventricular zone (V-SVZ), neural stem cells (NSCs) give rise to transit-amplifying progenitor (TAP) cells. These progenitors reside in different subniche locations, implying that cell movement must accompany lineage progression, but the dynamic behaviors of adult NSCs and TAPs remain largely unexplored. Here, we performed live time-lapse imaging with computer-based image analysis of young and aged 3D V-SVZ wholemounts from transgenic mice with fluorescently distinguished NSCs and TAP cells. Young V-SVZ progenitors are highly dynamic, with regular process outgrowth and retraction and cell migration. However, these activities dramatically declined with age. An examination of single-cell RNA sequencing (RNA-seq) data revealed age-associated changes in the *Rho-Rock* pathway that are important for cell motility. Applying a small molecule to inhibit ROCK transformed young into old V-SVZ progenitor cell dynamic behaviors. Hence RHO-ROCK signaling is critical for normal adult NSC and TAP movement and interactions, which are compromised with age, concomitant with the loss of regenerative ability.

INTRODUCTION

The adult murine ventricular-subventricular zone (V-SVZ) contains neural stem cells (NSCs) that sustain lifelong neurogenesis (Gage and Temple, 2013; Silva-Vargas et al., 2013). Prior work revealed an intricate 3D architecture in the V-SVZ. The germinal tissue is essentially sandwiched between two cell layers: the ependymal layer on the ventricular side and the vascular plexus on the striatal side (Shen et al., 2008; Tavazoie et al., 2008). Glial-fibrillary acidic protein (GFAP)-expressing quiescent NSCs (qNSCs) have a distinctive radial structure spanning these two domains, with a short apical process protruding into the ventricular space, a cell soma near the ependymal layer, and a long basal process contacting the vascular plexus. In contrast, immediate products of qNSCs, activated NSCs (aNSCs) expressing epidermal growth factor receptor (EGFR) and transit-amplifying progenitor (TAP) cells expressing achaete-scute homolog-1 (ASCL1) or MASH1 are found close to the vascular layer (Shen et al., 2008; Tavazoie et al., 2008). There, they give rise to neuroblasts that, by chain migration, eventually exit the V-SVZ en route to the olfactory bulb. We can then deduce that with lineage progression, there must be movement of NSCs and TAPs to different subniches within the V-SVZ, between the ependymal zone and the vascular zone.

Time-lapse studies of brain slices derived from postnatal day 10–210 Nestin-EGFP mice, labeling largely neuroblasts (68%), some ependymal cells (18%), and a minority of NSCs (8%) and TAPs (8%), demonstrated local progenitor "exploratory" movements (Nam et al., 2007). Later studies of brain slices from young mice (1–2 months old) using live cell reporters and two-photon microscopy showed that young neuroblasts were highly motile but that *mGfap*$^{+}$ and *Ascl1*$^{+}$ V-SVZ cells were stationary over 2 h (James et al., 2011; Kim et al., 2009). This encouraged us to study the movements of adult NSCs and TAPs in more detail for a longer period of time and in a preparation that enabled us to study cell movements between ependymal and vascular subniches.

The V-SVZ niche is amenable to study as a tissue explant or a "wholemount" preserving the 3D relationships of cells. Prior *ex vivo* live-imaging of the V-SVZ wholemount from young postnatal (postnal day 21 [P21]–P35) mice over a 4-day period revealed that NSCs extended and retracted their lateral processes and occasionally shifted their basal process on the vascular surface (Obernier et al., 2018). Hence, these pioneering experiments underscore the need to investigate cell-type-specific motility; no studies to date have specifically examined the dynamic properties of co-identified NSCs and TAPs in the adult V-SVZ, nor have they documented how these properties alter with age.

Several aging-related changes in V-SVZ composition have been reported, including decreased thickness (Luo et al., 2006), loss of total NSC numbers and ependymal cell coverage in males (Shook et al., 2012), and reactive phenotypes of ependymal cells and astrocytes (Capilla-Gonzalez et al., 2014). Also, with aging, NSC activity significantly reduces, with a loss of proliferation and reduced neuroblast

production (Luo et al., 2006). Surprisingly, TAP cell behavior does not follow the same trajectory: proliferation of TAPs declines from 6 to 8 months, but at 22 months, proliferation and cell-cycle reentry are increased (Apostolopoulou et al., 2017). These findings indicate that NSCs and TAPs show different responses to aging, likely reflecting their different roles in the stem cell lineage that demand specialized properties.

How adult V-SVZ progenitor cells move, interact, and transition to different zones is a key aspect of NSC and TAP niche biology that has remained largely unexplored due to several hurdles. These hurdles include the lack of a suitable live reporter system to visualize both cell types, problems encountered in preserving the adult 3D explant for prolonged periods *ex vivo*, which is exacerbated with an aged animal model, and the demand of quantifying large 3D time-lapse image datasets to build upon pioneering work in the V-SVZ (Nam et al., 2007). Here, we addressed this gap in our understanding of the dynamic properties of V-SVZ progenitor cells by generating a dual transgenic reporter mouse to distinguish NSCs and TAPs and an *ex vivo* culture system to enable the simultaneous tracking of both progenitor types over 20 h in 3D explants with time-lapse multiphoton microscopy, followed by computer-based image analysis. Further, we aged these animals to 28 months to investigate changes in V-SVZ NSC and TAP dynamic properties with aging.

Our studies on 3D V-SVZ wholemounts demonstrate that NSCs and TAPs in young adult animals are highly dynamic: for example, they constantly form and retract processes that exhibit exploratory behavior, while NSCs and TAPs migrate through the depth of the SVZ and regularly interact with each other. In contrast, with advanced age, NSCs and TAPs lose their dynamic properties and exhibit little process formation, and the large-scale movements characteristic of young progenitors are replaced by an enhanced membrane ruffling behavior.

To determine the molecular mechanism underlying age-related cell motility defects, we performed a bioinformatic analysis of motility-associated pathways in a single-cell RNA sequencing (scRNA-seq) dataset (Kalamakis et al., 2019) and found significant alterations in the *Rho-Rock* pathway in the V-SVZ NSCs and TAPs that were complex and cell-subtype-specific. Small-molecule inhibition of ROCK1/2 converted young NSC and TAP dynamic movements into those resembling the aged mouse, with significantly reduced process motility and cell migration, including in the z axis between the ependymal and vascular subniches. This loss of dynamism may contribute to age-related deficits in stem cell function that reduce the ability to repair and regenerate.

RESULTS

Live imaging of V-SVZ NSC and TAP reporter mice demonstrates dynamic movements and cell migration

In order to investigate the behavior of NSCs and TAPs in the V-SVZ niche, we bred the *hGFAP-GFP* mouse (Zhuo et al., 1997) with the *Ascl1-CreERT2/+ ; Ai9(RCL-tdT)* mouse (Kim et al., 2011; Madisen et al., 2010) to produce a double transgenic in which *GFAP-GFP*$^+$ (green) NSCs give rise to *Ascl1-cre x TdTomato (Ascl1-TdT)+* (red) TAPs. The *hGFAP-GFP* mice have been used to study adult V-SVZ NSCs with extensive validation, including cell purification and molecular characterization (Codega et al., 2014; Pastrana et al., 2009; Tavazoie et al., 2008). The *Ascl1-cre* mouse line has also been validated as a reporter to study V-SVZ TAPs, with functional analysis *in vitro* and lineage tracing *in vivo* demonstrating labeling of this TAP population (Kim et al., 2011; Mich et al., 2014). To confirm the cell identity in our double transgenic mice, 2 days after tamoxifen injection, we verified that most of the GFP$^+$ cells co-stained for GFAP (97%) and that most of the Tdtomato$^+$ cells co-stained for ASCL1 (67%); of the Tdtomato$^+$ cells that were ASCL1$^-$, around 15% were GFAP-GFP$^+$, consistent with these being early cells transitioning from NSCs to TAPs but not yet expressing detectable levels of the ASCL1 protein (Figure S1).

We developed an *ex vivo* culture system enabling continuous multiplex fluorescence imaging of the adult V-SVZ wholemount for over 20 h. Immediately after sacrifice, we dissected the V-SVZ wholemount and stained it with isolectin to label ependymal cells and blood vessels, which allows us to use these two niche layers as references for the location of NSCs and TAPs as they move within the tissue (Figure 1A). Stained explants were mounted in a perfusion system circulating an optimized culture medium equilibrated with 40% O_2 and 5% CO_2 (see experimental procedures and supplemental experimental procedures), which maintains long-term viability while recording progenitor cell movements with scans taken every 9 minutes (Figure 1B). An image projection shows the whole area of the niche examined (Figure 1C′). Note that blood vessels (Figure 1C″) and ependymal cells (Figure 1C‴) labeled with isolectin are clearly distinguishable by morphology as well as by image plane. We focused on the anterior dorsal region of the V-SVZ explant, a region studied for its active neurogenesis and close apposition to the rostral migratory stream (Law et al., 1999), because our prior work demonstrated the presence of NSCs and TAPs and of chains of migrating neuroblasts in this area in both young and aged animals (Zhao et al., 2021).

We first examined the morphologies of NSCs and TAPs in the V-SVZs of young (2- to 3-month-old) mice (Figure 1D). Reconstructed 3D images show that NSCs close to the ependymal zone often have a flattened soma, a short apical

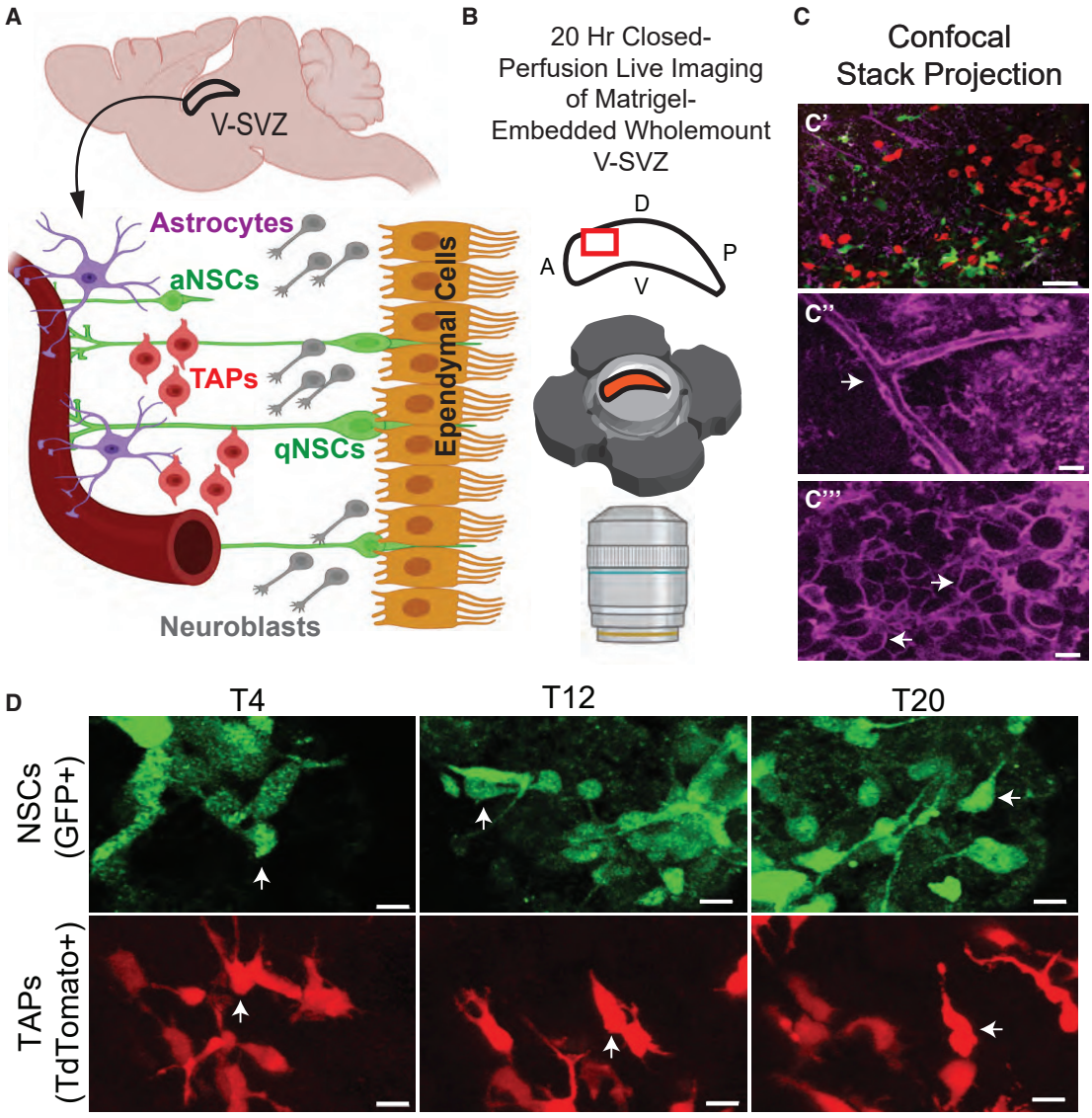

Figure 1. Time-lapse recording of the 3D V-SVZ wholemount from transgenic mice with *GFAP*-GFP + NSCs and *Ascl1*-TdTomato + TAPs

(A) Diagram of the V-SVZ with progenitors located between the ventricular ependymal layer and the vascular plexus.

(B) Schematic. Top: red rectangle indicates the anterior dorsal region imaged. A, anterior; P, posterior; D, dorsal; V, ventral. Bottom: Matrigel-embedded V-SVZ in imaging chamber.

(C) Representative images of different optical layers of the wholemount preparation to illustrate distinct cell morphologies: (C′) NSCs (green), TAPs (red); (C″-C‴) lectin (purple) staining reveals the deep vasculature (C″ arrow) and the superficial ependymal cells (C‴, arrows indicate examples). Scale bar, 40 μm (C′) and 5 μm (C″ and C‴).

(D) Image sequences from a 2-month-old animal at times (T) 4, 12, and 20 h illustrate dynamic movements. White arrows indicate the same cell at different timepoints. Scale bar, 5 μm.

See also Figure S1 and Videos S1, S2, S3, and S4.

process, and a long basal process extending through the depth of the V-SVZ to contact blood vessels (Mirzadeh et al., 2008; Shen et al., 2008; Tavazoie et al., 2008). In young mice, live-imaged NSCs indeed exhibited short and long processes, which were surprisingly dynamic, showing frequent extensions and retractions (Video S1), and they displayed membrane ruffling and extensive cell-cell contacts (Video S2). TAPs in young animals were, as expected, more abundant deeper in the V-SVZ than were NSCs, and many had one or two long processes showing frequent extensions

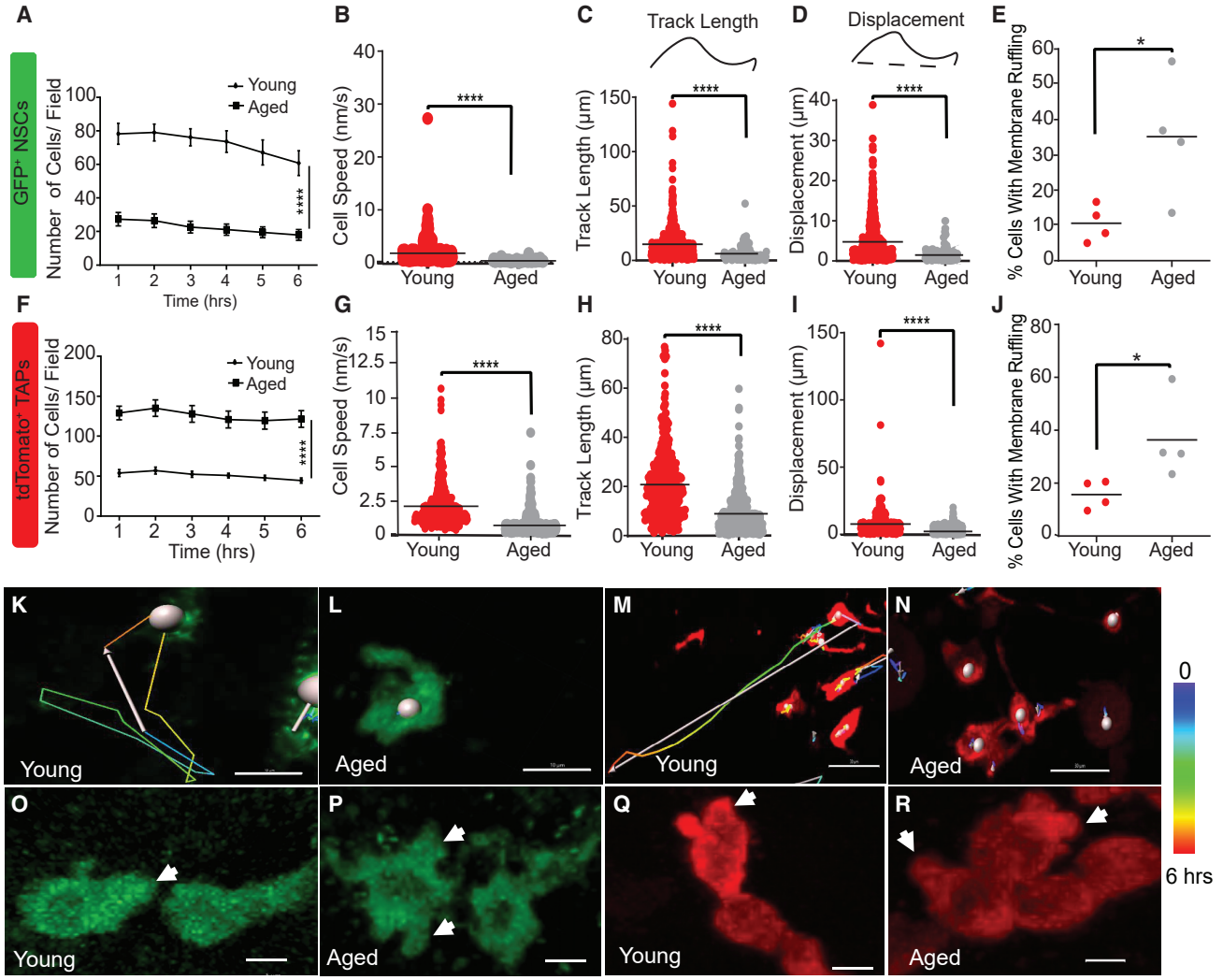

Figure 2. Time-lapse recording of the 3D V-SVZ revealed NSCs and TAPs become less motile with age

Analyses of 6 h of timelapse recording of V-SVZ 3D wholemounts are shown.

(A–D) Aged male mice have fewer GFP + NSCs, but numbers remained stable over the analysis period (A), while travel speed (B), distance traveled (track length) (C), and displacement of NSCs (D) significantly decreased with age.

(E) Aged NSCs showed more membrane ruffling.

(F–I) Aged mice have more TAPs, but numbers remained stable over the analysis period (F), while travel speed (G), distance traveled (track length) (H), and displacement of TAPs (I) significantly decreased with age.

(J) Aged TAPs showed more membrane ruffling.

(A and F) Mean ± SEM, two-way ANOVA ****$p < 0.0001$. (E and J) Student's t test *$p < 0.05$. (B–D and G–I) Kolmogorov-Smirnov (KS) test determining population-level differences between groups; ****$p < 0.0001$. Values in parentheses indicate cell numbers in young versus aged animals: (B–D) n = (561, 116) and (G–I) n = (348, 633). (B–E and G–J) Graph bars indicate mean. n = 4 mice/group.

(K–R) Representative images of aged and young cell migration for NSCs (K and L) and TAPs (M and N) and of ruffling for NSCs (O and P) and TAPs (Q and R).

(K–N) White spot indicates cell body, spectrum-colored line indicates the time during imaging (key on right), and arrow indicates track length and displacement.

(O–R) Arrows indicate examples of ruffles.

Scale bar, 10 µm (K and L), 30 µm (M and N), and 5 µm (O–R).

See also Figure S2 and Videos S2, S4, S5, and S6.

and retractions (Video S3) and they displayed membrane ruffling (Video S4). Young NSCs and TAPs often had a unipolar or bipolar morphology with a leading process, similar to the morphology described for neuroblasts in the V-SVZ (De Marchis et al., 2001), and were migratory (Figure 1D). Hence, in the adult V-SVZ, both NSCs and TAPs showed highly dynamic phenotypes. Given these observations, we asked how the morphology, motility, and migration of V-SVZ progenitor cells were altered with aging by quantifying these dynamic properties.

V-SVZ NSC and TAP dynamism is impaired with age

To examine age-related changes in NSC and TAP cell dynamic behaviors, we time-lapse-recorded whole-mount V-SVZs dissected from young (2- to 3-month-old) and aged (27- to 28-month-old) animals. We collected one movie from each V-SVZ preparation then segmented the movies and analyzed the dynamic properties of the NSCs and TAPs in each frame of each image per V-SVZ using Imaris software. We used the spot module, which tracks cell body movements, to analyze NSC and TAP cell migration (Figure 2; Figures S2A–S2C).

As described previously (Shook et al., 2012), the number of NSCs in the male mouse V-SVZ was lower in aged animals but remained relatively stable over the first 6 h of imaging (Figure 2A), so we focused on this time frame for most of our analyses. We noted a dramatic loss of process production and NSC motility with aging (Video S5). The average migration speed of young NSCs was 1.8 nm/s, which decreased to 0.3 nm/s in aged mice (Figure 2B). Given that neuroblasts often change direction while migrating (James et al., 2011; Schaar and McConnell, 2005), we measured the total track length traveled by individual NSCs as well as the total distance between the first and last position of the cell (track displacement) during the 6-h period. In young mice, NSCs were motile by both measures: the average total travel distance and track displacement were 15 and 4.8 μm, respectively (Figures 2C and 2D). In aged mice, however, both parameters decreased significantly to 6.3 and 1.5 μm, respectively, revealing a dramatic reduction in NSC migration with age. Rather than active process extension and movement, aged NSCs displayed significantly more membrane ruffling compared with young NSCs (Figure 2E; Video S2). In contrast, the number of NSCs with processes was significantly lower in aged mice (Figure S2D).

We found that the number of TAPs increased with age in the anterior V-SVZ (Figure 2F). Previously, we showed that TAP cell proliferation is dysregulated with aging so that the number of proliferative *Ascl1*$^{+}$ cells in the mouse V-SVZ increased from 18 to 22 months of age (Apostolopoulou et al., 2017). These data indicate that this trend continues so that by 27 to 28 months of age, there are more TAPs even than in young adult animals. Nevertheless, despite a greater number of TAPs, there was a dramatic decrease in TAP migration speed with age, with a mean of 2.1 nm/s in young mice and 0.7 nm/s in aged mice (Figure 2G and Video S6). In young mice, TAPs were highly active and motile, showing frequent cell body translocations. The average total travel distance and track displacement of TAPs were 20.8 and 7.7 μm, respectively, over the 6-h recording period. In contrast, aged mice showed a dramatic reduction in TAP migration (travel distance: 8.9 μm; displacement: 2.2 μm) (Figures 2H and 2I). Aged TAPs were largely stationary but exhibited extensive membrane ruffling, greater than in young mice (Figure 2J; Video S4), and the number of aged TAPs with cell processes was significantly less than in young mice (Figure S2D). Representative images indicating NSC and TAP cell migration and membrane ruffling in young and aged mice are shown in Figures 2K–2R.

Migration between ependymal and vascular zones and interactions between NSCs and TAPs decreased with age

qNSCs reside largely within 5 μm of the ependymal zone, while aNSCs and TAPs are present closer to the vasculature, frequently about 15 to 20 μm below the ependymal surface (Shen et al., 2008). In order to transition between lineage compartments, somal movement is implied, but to date, this migration between ependymal and vascular subniches has not been documented. Therefore, we calculated the somal movements of NSCs and TAPs in the z axis of the V-SVZ wholemount from approximately 5 to 20 μm below the ependymal zone. We found that both progenitor types moved in the z axis (x = 1.4 μm NSCs and 1.7 μm TAPs); however, they moved significantly less with aging (x = 0.6 μm NSCs and 0.7 μm TAPs) (Figure 3A). NSCs and TAPs move in both directions in the z axis, but, with age, their directional z movements were reduced and biased toward moving deeper into the tissue, away from the ependymal zone, and toward the vasculature (young versus aged, x: NSCs, 0.2 vs –0.4 μm; TAPs, 0.1 versus –0.2 μm) (Figure 3B).

Given that NSCs and TAPs both move in the z axis providing the opportunity to make contact, we examined their interactions and how these change with age. In young mice, NSCs and TAPs frequently extend cell processes, contact each other's cell processes or soma, and then retract their processes, consistent with exploratory behavior. We often observed these direct interactions just before a large cell body translocation (Video S7). Direct cell-cell interactions are critical for collective cell migration (Mishra et al., 2019), but how NSCs and TAPs communicate and

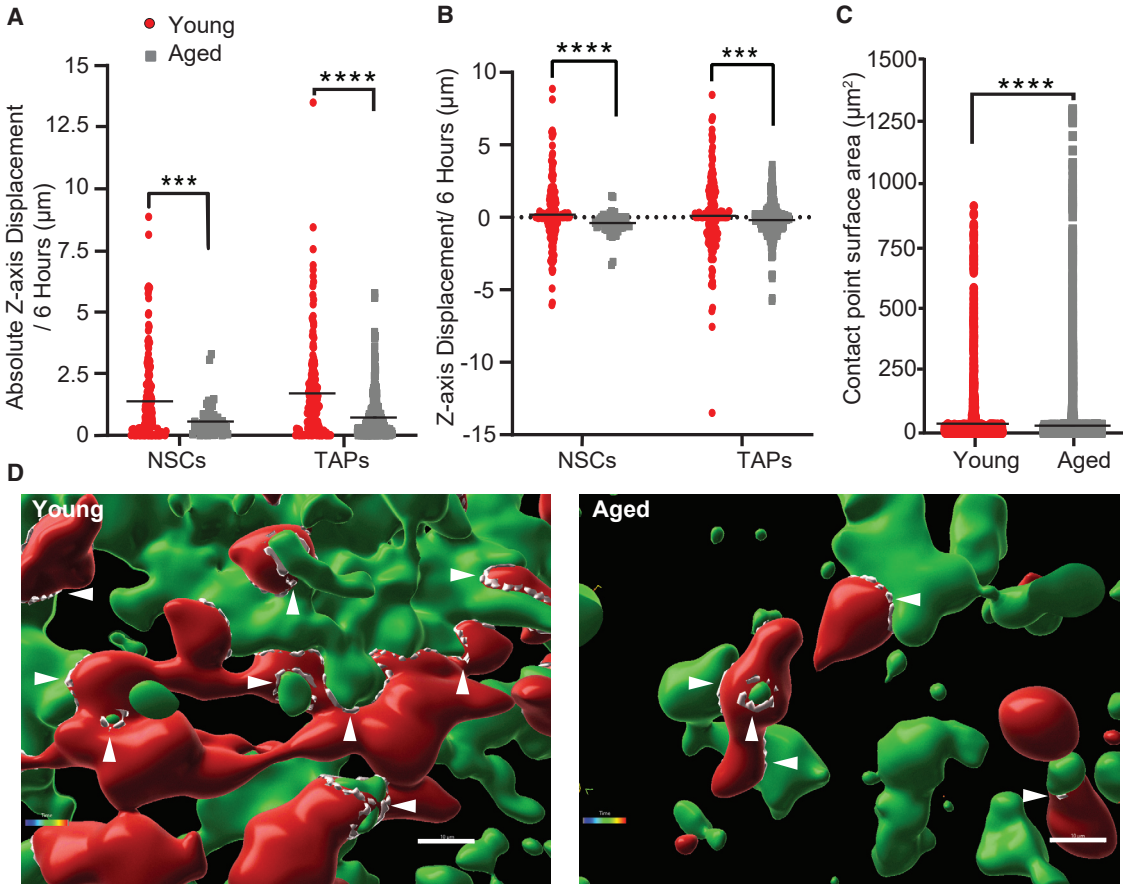

Figure 3. Travel in the z axis between the ependymal and vascular subniches significantly reduces with age

(A) Total distance moved by NSCs and TAPs in the z axis of the niche is less with age.

(B) Young NSCs and TAPs move in both directions in the z axis. With age, motility is reduced and NSCs and TAPs move closer to the vasculature (0 = start position, +ve versus –ve values = movement to or away from the ependymal layer).

(C) Surface contact area between NSCs and TAPs over 4 h significantly declined with age.

(A–C) KS test, ***p < 0.001, ****p < 0.0001. Graph bars indicate the mean. Values in parentheses indicate cell numbers in young versus aged animals: n = NSCs: (207, 57) and TAPs: (166, 399). Cell-cell interactions n = (4,577, 9,290). n = 4 mice/group.

(D) Representative rendered images showing interactions between NSCs (green) and TAPs (red) in young and aged V-SVZs. Surface contact area indicated by white dotted lines, and arrowheads show examples. Scale bar, 10 μm.

See also Video S7.

how aging affects communication remain largely unknown. Using Imaris XTension, we measured the interactions of NSCs and TAPs over the first 4 h of time-lapse recording. In young animals, NSCs and TAPs contacted each other extensively, but with aging, this was significantly reduced by approximately 25% (from x = 37.9 to 28.3 μm^2) (Figures 3C and 3D).

The *Rho-Rock* pathway changes with age in NSCs and TAPs

Given the profound changes in the motility of NSCs and TAPs in the aged V-SVZ, we wanted to determine which genes or pathways may underlie this observation. A recent study performed scRNA-seq on cells in young and old V-SVZs (Kalamakis et al., 2019), which we used as a resource to determine cell-type-specific gene expression changes with aging. This paper identified seven transcriptionally unique cell types: five NSC subtypes, including two populations of qNSCs (qNSC1 and qNSC2), and three populations of aNSCs (aNSC0, aNSC1, and aNSC2), as well as TAPs and neuroblasts (Figure 4A). We intersected the significantly altered genes in old versus young animals with those in the Gene Ontology (GO) pathway entitled "cell migration" and cross-referenced the identified genes to Reactome pathways to determine the pathways significantly enriched in each cell subpopulation.

We found several progenitor cell subtypes demonstrated enrichment in at least one *Rho*-related pathway that

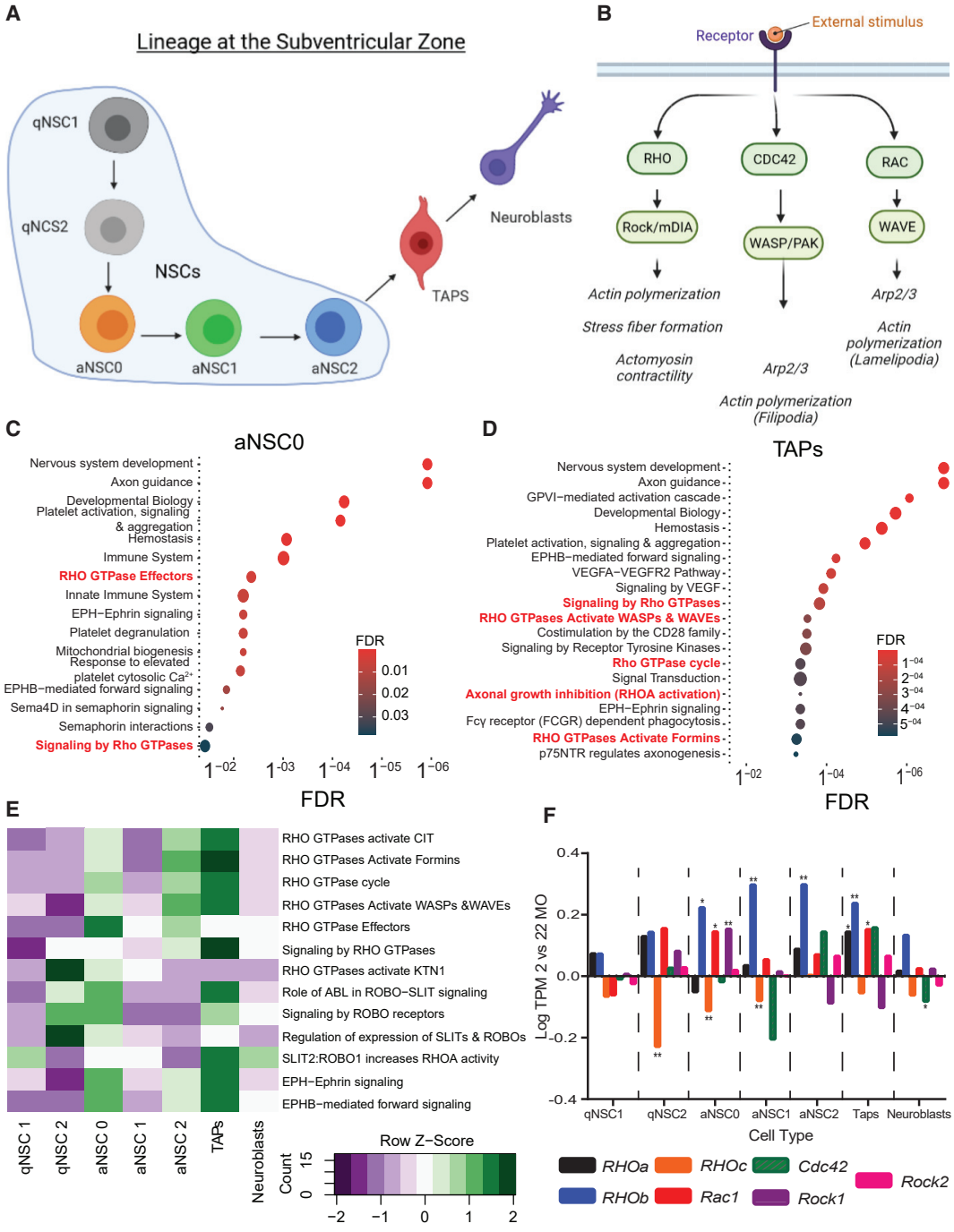

Figure 4. Age-related gene expression changes in V-SVZ progenitor subtypes highlight *Rho* motility pathways

(A) Lineage relationships of progenitor cells identified in the V-SVZ (Kalamakis et al., 2019).

(B) Schematic of RHO GTPases, downstream effectors, and their motility functions.

(C and D) Reactome pathways enriched in aged (22-month-old) compared to young (2-month-old) V-SVZs. *Rho* pathways highlighted in red for aNSC0 (C) and TAPs (D).

(E) Heatmap of selected pathways in old versus young V-SVZs shows differences between cell types.

(F) Changes in expression of *Rho*, *Rock*, *Rac*, and *Cdc42* genes in old versus young V-SVZ progenitor cell subtypes (TPM, transcripts per million reads). *p <0.05, **p <0.01, values as used in Table S2 in Kalamakis et al., (2019).

See also Figures S3 and S4 and Table S1.

changed with aging. As *Rho* GTPases are involved in cellular migration, process extension, and membrane ruffling (Figure 4B), their differential expression in NSCs and TAPs may contribute to the dynamic properties and aging phenotypes that we observed. Interestingly, we saw age-associated enrichment for multiple *Rho* pathways in aNSC0s (Figure 4C), TAPs (Figure 4D), and qNSC2s (Figure S3), which may indicate that these pathways are more impacted by aging in certain phases of the lineage. (For more information on the genes in each pathway identified and pathways enriched for each cell type, see Table S1.)

To establish in more detail the progenitor cell-type-dependent changes in the V-SVZ with aging, we analyzed the magnitude of change in differentially expressed genes in several *Rho* signaling pathways (Figure 4E). We found that TAPs show the most increased expression of *Rho* signaling genes in old versus young mice, followed by aNSC0s. Interestingly, although aNSCs progressed from aNSC0 to aNSC1 then to aNSC2 in the Kalamakis study (Figure 4A), pathways were notably upregulated in aNSC0 and aNSC2 but not in aNSC1, suggesting unique requirements for motility within each cell subtype of the lineage.

To examine gene expression in migration-related pathways in more detail, we plotted the change in gene expression in old versus young mice (Figures 4F and S4). With aging, there was an upregulation of *Rhob* and *Rhoa* and a reduction of *Rhoc* across most of the cell subclasses. While most genes changed in the same direction within each cell type, there were several instances where genes were differentially altered across cell types, for example, *Cdc42*, *Rock1*, and, to a lesser extent, *Rock2*. While these different effectors have all been implicated in migration, their increased or decreased expression can promote or inhibit cell movement depending on cell type, cell context, and environment. Hence, it is important to empirically test the impact. Given the significant changes in *Rho* pathway components with aging, we examined whether this pathway was involved in regulating dynamism of V-SVZ progenitor cells.

ROCK inhibition decreases the motility of young NSCs

To test our hypothesis that altered RHO-ROCK GTPase signaling could adversely affect V-SVZ progenitor cell motility, we applied 40 μM Y27632, a selective ROCK1/2 inhibitor (ROCKi), to young wholemount V-SVZs and monitored its effect over 6 h in NSCs (Figures 5A–5D) and TAPs (Figures 5E–5H). There was no significant difference in the number of NSCs or TAPs when comparing ROCKi to vehicle control (Figures 5A and 5E), indicating that ROCKi did not affect cell survival or proliferation over this period. Although most NSCs and TAPs still displayed a migratory morphology with a leading process and a trailing edge after ROCKi treatment, similar to their morphology in vehicle (DMSO) control, they showed a significantly reduced average speed of migration (NSCs: 1.2 to 0.9 nm/s; TAPs: 1.5 to 0.8 nm/s), distance traveled (NSCs: 14.6 to 11.1 μm; TAPs: 21.9 to 12.5 μm), and displacement (NSCs: 6.1 to 4.2 μm; TAPs: 7.4 to 4.9 μm) (Figures 5B–5D for NSCs and 5F–H for TAPs).

To determine if ROCKi could mimic age-related changes in the movement between ependymal and vascular compartments, we measured the total distance traveled by NSCs and TAPs along the z axis. After applying ROCKi, NSCs moved less in the z axis (x= 2.5 versus 1 μm) (Figure 6A) and showed a bias away from the ependymal layer towards the vasculature (x= 2.0 versus 0.0 μm) (Figure 6B), mimicking the behavior of aged NSCs (Figure 3B). TAPs treated with ROCKi moved less in the z axis (x = 2.2 versus 1.6 μm) (Figure 6A) and also moved deeper into the V-SVZ, closer to the vasculature (x = 1.4 versus −0.9 μm) (Figure 6B), as with aging. NSCs and TAPs still interacted with each other, and the measured area of cell-cell contact between them was increased (x = 27.4 μm^2 vehicle versus 50.7 μm^2 ROCKi) (Figures 6C and 6D), likely because ROCKi caused increased cell crowding, which enabled more interactions. In summary, ROCKi applied to young V-SVZ wholemounts dramatically reduced progenitor migration and distance traveled and altered their movements in the z axis between the ependymal to vascular compartments, all together mimicking their reduced motility in the aged V-SVZ.

DISCUSSION

In the adult V-SVZ, dynamic properties of the two major progenitor cell types, NSCs and TAPs, have not been comprehensively examined or quantified. Here, we investigate this using 4D analysis by time-lapse recording of the adult 3D V-SVZ wholemount that preserves much of the niche architecture. We revealed that with aging, there are major deficits in NSC and TAP motility, process production and retraction, migration between subniches, and cell-cell interactions. Moreover, we identify changes in *Rho-Rock* signaling pathways occurring with aging and show that ROCKi can transform young NSC and TAP behaviors into those characteristic of old mice. Hence, this study reveals, for the first time, the dynamic movements of NSCs and TAPs in the adult V-SVZ, shows that these are dramatically compromised with aging, and highlights an underlying molecular pathway involved in progenitor cell movement that changes significantly with aging in a cell-type-dependent manner.

Our studies show that NSC processes are highly motile in the young V-SVZ, exhibiting frequent extensions and retractions. This adds to prior findings made in juvenile

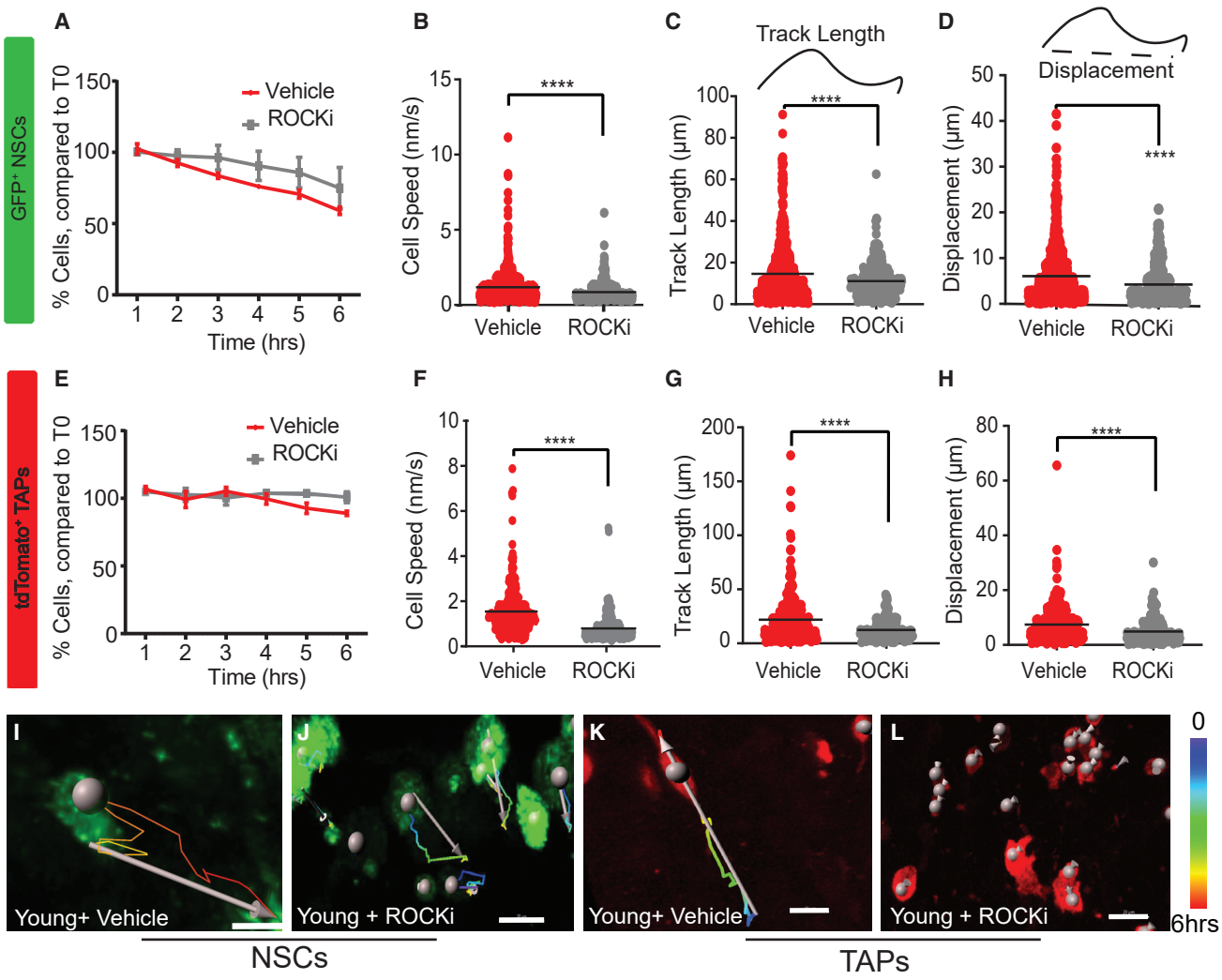

Figure 5. ROCKi decreased progenitor cell motility in the young V-SVZ

(A–D) ROCKi did not change the number of NSCs in each field over the 6-h recording period versus vehicle (DMSO) but significantly decreased NSC travel speed (B), distance traveled (C), and displacement (D).

(E–H) ROCKi did not change the number of TAPs (E) but significantly decreased TAP migration speed (F), distance traveled (G), and displacement (H).

(A and E) Two-way ANOVA, n = 3 mice/group. (B–D and F–H) KS test, ****$p < 0.0001$. Graph bars indicate the mean. Values in parentheses indicate cell numbers (vehicle, ROCKi): (B–D) n = (637, 342) and (F–H) (300, 207).

(I–L) Representative images: NSCs from vehicle (I) and ROCKi (J) and TAPs from vehicle (K) and ROCKi (L) groups. A white spot labels each cell body, the spectrum-colored line indicates time during imaging (key on right), and arrow indicates track displacement over 6 h. Scale bar, 10 µm (I and J) and 20 µm (K and L).

mice that NSC lateral processes can extend and retract and that the endings of a long basal process can move along V-SVZ blood vessels (Obernier et al., 2018). As NSCs become activated and express EGFR, their position in the niche changes to be nearer to V-SVZ blood vessels (Shen et al., 2008). This implies that NSCs move their soma from the ependymal to the vascular niche upon activation. Here, we show that NSCs do indeed move between the ependymal and vascular layers and, moreover, that their movements are not unidirectional, but that the cells move back and forth in the z axis.

TAPs tend to be located near the V-SVZ vascular plexus where they proliferate and produce neuroblast progeny that join the rostral migratory stream. We show that TAPs, like NSCs, can be uni- or bipolar and that they also actively extend and retract processes. Young TAPs migrate actively in the V-SVZ, including in the z axis in both directions, and can directly interact with NSCs

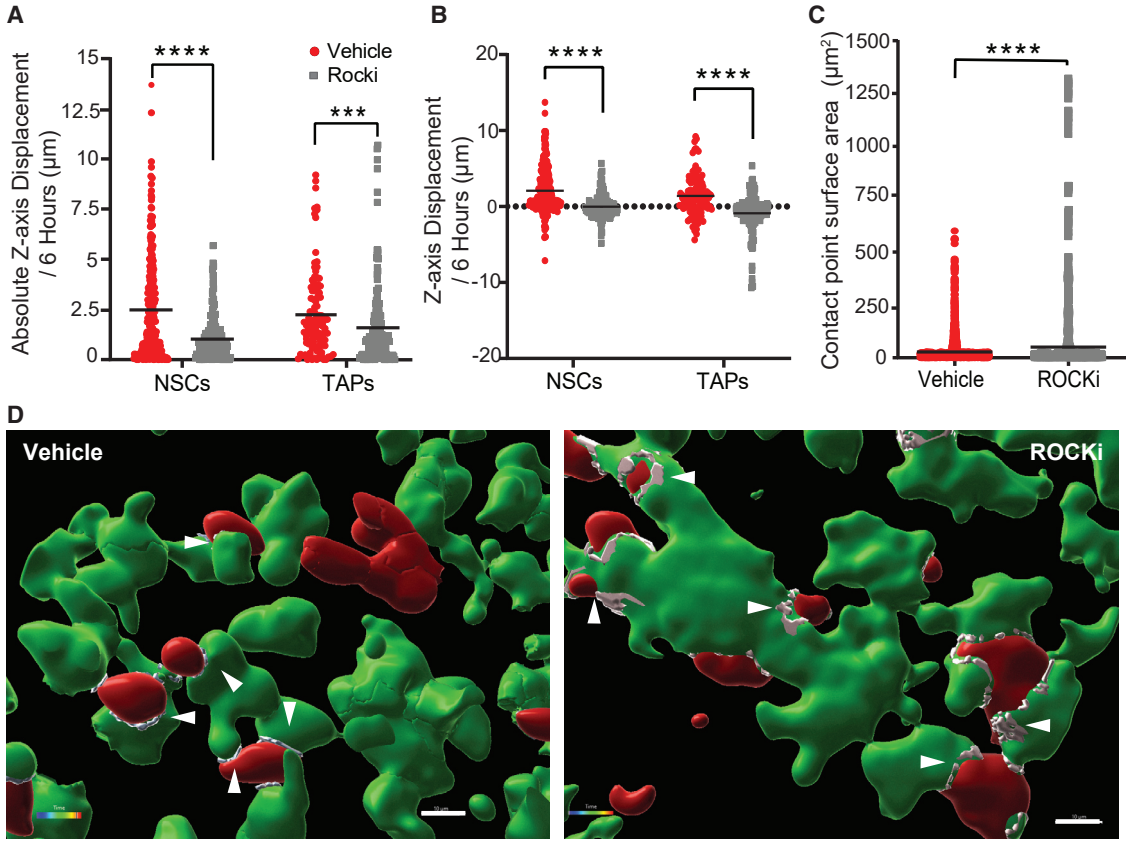

Figure 6. ROCKi reduces young V-SVZ NSC and TAP cell movement

(A) ROCKi significantly reduced total travel distance in the z axis.

(B) ROCKi caused NSCs and TAPs to move deeper (more –ve z axis displacement, 0 = starting position).

(C) Surface contact area between NSCs and TAPs over 4 h of recording was significantly increased by ROCKi.

(A–C) Values in parentheses indicate cell numbers: (vehicle, ROCKi): n = NSCs: (256, 152), TAPs: (112,164), and (C) (2,588, 2,168). (A–C) Graph bars indicate the mean. KS test ****$p < 0.0001$, ***$p < 0.001$. n = 3 mice/group.

(D) Representative rendered images show interactions between NSCs (green) and TAPs (red) in vehicle- and ROCKi-treated V-SVZs. Surface contact shown in white, and examples are indicated with arrowheads. Scale bar, 10 µm.

either via their contacting processes or cell bodies. Such contacts sometimes precede a large somal movement, and it will be fascinating to examine the effects of these progenitor cell-cell contacts and molecular cross-communications.

Prior studies on young postnatal V-SVZ progenitor cells, focused largely on neuroblasts, have recorded speeds of 5 to 20 nm/s (James et al., 2011). In our measures from 2-month-old adult wholemounts, the mean migration speed is ~1 nm/s for NSCs and ~1.4 nm/s for TAPs. Given these measurements include both motile and non-motile cells, we then analyzed the dynamic properties of young motile NSCs and TAPs, defined by cells with a total track length of ≥20 µm during the 6-h recording period (Figures S2A–S2C). Young motile NSCs had an average speed of 3.1 nm/s, an average track length of 32.2 µm, and a displacement of 9.1 µm. Young motile TAPs moved at a speed of 2.5 nm/s, with a total track length of 35.6 µm and a displacement of 11.6 µm. Hence, even when considering only motile cells, NSCs and TAPs move slower than migrating neuroblasts. Differences in recording parameters could also contribute to differences in migration speed and other aspects of motility.

Our observation of considerable dynamism in young adult V-SVZ NSCs and TAPs prompts the question about its role in normal lineage progression. Prior studies have shown that the ependymal layer releases factors such as pigment epithelium-derived factor (PEDF) that are important for progenitor maintenance (Ramirez-Castillejo et al., 2006), while the V-SVZ vasculature produces signals such as SDF1 and VEGF-C that stimulate proliferation and neurogenesis (Matta et al., 2021; Zhu et al., 2019). The bidirectional movement of both NSCs and TAPs in the z axis in young animals between the ependymal and vascular zones

may impact signals they receive from these subniches, as well as from each other, and thus their eventual commitment to a specific behavior. In the future, it will be interesting to examine whether NSCs also show dynamic changes between states of activation and quiescence as they move between the ependymal and vascular subniches.

With aging, we found a significant loss of dynamic movements in both NSCs and TAPs. Aged NSCs lacked the characteristic morphology of migrating cells, with a leading process and a trailing edge (De Marchis et al., 2001), and exhibited increased ruffling. Similarly, aged TAPs became less process-bearing and typically stayed in place while exhibiting a strong membrane ruffling behavior. Lack of normal process-bearing morphology may contribute to lack of migration given that, in other cell types, the leading process establishes contacts with the extracellular matrix and the nucleus then translocates towards the centrosome and induces somal movements (Schaar and McConnell, 2005). When the membrane process fails to establish focal adhesions, it retracts, and membrane ruffles form (Borm et al., 2005). It is possible that increased membrane ruffling reflects a failure to form focal adhesions in the inflammatory environment present in the aged V-SVZ (Cutler and Kokovay, 2020).

Our examination of single V-SVZ cell gene expression pathways that significantly changed with aging (Kalamakis et al., 2019) highlighted the *Rho* pathway. RHO GTPases orchestrate key steps during cell migration (Guan et al., 2020; Ridley, 2015) and are part of the non-canonical Wnt pathway, which decreases with age in the V-SVZ (Kalamakis et al., 2019). We found that different cells in the NSC lineage showed distinct changes in *Rho* gene expression with aging. All cells in the lineage showed an increased level of *RhoB* with aging, which is interesting given that RHOB has been reported to increase expression and activity in macrophages and endothelial cells in inflammatory situations (Vega and Ridley, 2018). If this is part of an aging or inflammatory response, it will be worthwhile investigating the impact of increased *RhoB* in these aged neural progenitor populations. Activated RHOB has several effects on cells: it is localized to endosomes, is important for intracellular trafficking, and can drive increased endosomal association with actin filaments, thus preventing the normal transport of receptors, including EGFR (Fernandez-Borja et al., 2005; Wherlock et al., 2004). This may be significant in the context of the aging V-SVZ niche because EGFR is expressed on both aNSCs and TAPs and regulates their proliferation and migration (James et al., 2011; Kim et al., 2009). Moreover, RHOB is important for cytokine-receptor trafficking and chemotaxis. Given that we have found aNSCs express the CXCR4 receptor and show chemotaxis towards SDF1 released from vascular endothelial cells (Kokovay et al., 2010; Zhu et al., 2019), it is conceivable that altered RHOB function could contribute to the impaired directional cell movements we observed with aging. Higher levels of RHOB can also inhibit cell migration and proliferation and promote apoptosis (Vega and Ridley, 2018), which may explain additional aging phenotypes documented in the V-SVZ.

Several progenitor cell types show upregulation of *RhoA*, which, like *RhoB*, can inhibit migration at increased levels, although an excessive depletion of *RhoA* can also inhibit migration, implying that a critical level is required (Ridley, 2015). Examining molecules that modify the RHOA function, including RND2 and RND3, which suppress RHOA, MST3, which phosphorylates RHOA to reduce its activity, and CCM3, which decreases RHOA activation (Pacary et al., 2011), we again found cell-type-specific gene expression changes with aging (Figure S4). Most progenitor cells showed a downregulation of *RhoC*; despite being highly similar to *RhoA*, reduced or depleted RHOC has been associated with reduced cell migration, loss of polarization, and increased numbers of lamellipodia (Vega et al., 2011). These alterations could contribute to the loss of a process-bearing morphology and the increased ruffling behavior we saw in aged V-SVZ progenitor cells. We found that in early stage NSCs, *Rock1* increases with aging, but in later stage aNSCs and TAPs, it decreases. TAPs are further distinct from NSCs in having higher levels of *Rac1* and *Cdc42* with aging. Increased *Rac1* can act synergistically with *Cdc42* to cause increased membrane ruffling (Kurokawa et al., 2004), which was pronounced in aged TAP cells. Interestingly, neuroblasts derived from TAPs do not show notable changes in *Rho*, *Rac*, or *Cdc42* with aging. These complex observations show the importance of examining these pathways and how they change with age and impact dynamic movements on a cell-subtype level.

Prior studies focused on neuroblasts have shown that ROCKi increased the chain migration of progenitor cells derived from P3 mouse V-SVZ explants and enhanced the migration of V-SVZ-derived polysialylated neuronal cell adhesion molecule (PSA-NCAM)+ cells but disrupted their normal direction into the olfactory bulb in adult mice *in vivo* (Leong et al., 2011). In our studies, we found the opposite result on NSC and TAP migration: applying ROCKi to the young V-SVZ significantly reduced NSC and TAP migration speed and travel distance compared with vehicle control. This difference in progenitor cell-type responses underscores that the correct level of signaling in the RHO-ROCK pathway is important for normal NSC, TAP, and neuroblast motility in a cell-type-dependent manner.

Although NSCs and TAPs were inhibited from moving after ROCKi, they still demonstrated a process-bearing morphology. As discussed above, RHO GTPases control somal translocation via ROCK (Ota et al., 2014). However, membrane protrusion and retraction at leading processes are mainly regulated by RAC and CDC42 GTPases mediating actin dynamics (Leong et al., 2011). ROCKi can induce robust neurite outgrowth, accompanying rapid cofilin dephosphorylation (Zhang et al., 2006). We conclude that while reduced RHO-ROCK signaling might contribute to reduced cell dynamism in the aging niche, other pathways are responsible for the loss of processes seen in aged V-SVZ progenitor cells, likely involving RAC1 and CDC42 imbalances. Our finding that ROCKi transformed several young into old V-SVZ progenitor cell dynamic behaviors encourages us that further exploration of motility-associated pathways could identify additional small molecules that impact specific behaviors, with the eventual goal of preventing age-associated loss of cell dynamism in the niche.

EXPERIMENTAL PROCEDURES

Please see more details provided in supplemental experimental procedures.

Animals

hGFAP-GFP transgenic mice *(FVB/N-Tg(GFAPGFP)14Mes/J*, Jackson Laboratory) were crossed with *Ascl1-Cre-Tomato mice (Ascl1tm1.1 (cre/ERT2); B6.Cg-Gt(ROSA)26Sortm9(CAG-tdTomato) Hze/J*, Jackson Laboratory) (Kim et al., 2011). Male *Ascl1<CreERT2/+>; R26R<tomato/tomato/+>; GFAP<GFP/+>* offspring were aged as needed. Procedures were approved by the Institutional Animal Care and Use Committee at SUNY Albany.

Tamoxifen (TAM) treatment

TAM (Sigma, T5648-5G) was prepared as a 30 mg/mL stock solution in ethyl alcohol (Sigma, E7023) and diluted 1:10 in sunflower seed oil (Sigma, S5007). Two days before use, animals were injected intraperitoneally with a single dose of 180 mg/kg TAM.

V-SVZ wholemount preparation and immunohistochemistry (IHC)

The V-SVZ was dissected as described (Shen et al., 2008), fixed in 4% paraformaldehyde (4% PFA) for 45 min, and rinsed 3 times with phosphate-buffered saline (PBS) prior to IHC. One V-SVZ/mouse (hemisphere chosen at random) was selected for IHC.

IHC

Wholemounts were incubated for 1 h in 0.5% triton-X in PBS (TPBS) then in 10% normal donkey serum (NDS; Jackson ImmunoResearch, 017000121) in TPBS for 1 h. Primary antibodies were incubated overnight at 4°C; for NSCs: chicken anti-GFP (1:100; Rockland, 600-901-215), rat anti-GFAP (1:500; Invitrogen, 13-0300) and for TAPs: rabbit anti-MASH1 (ASCL1) (1:100; Abcam, ab211327) in TPBS. After rinsing 3 times with TPBS, secondary antibodies (Jackson ImmunoResearch) were added at 1:300 in TPBS: donkey anti-chicken immunoglobulin G (IgG) 488 (703545155), donkey anti-rat IgG CY5 (712605153) (for NSCs), or donkey anti-rabbit (711605152) (for TAPs). Wholemounts were then washed 3 times with TPBS and incubated with DAPI (1:1,000; Invitrogen, D1306) for 10 min at room temperature (RT). After rinsing 3 times with TPBS, V-SVZs were mounted on glass slides with tissue spacers in Prolong Gold Antifade reagent with DAPI (Invitrogen, P366931).

V-SVZ wholemount preparation and live imaging

V-SVZ wholemounts were dissected in ice-cold adult hibernation buffer (supplemental experimental procedures). Samples were stained with isolectin (Thermofisher Scientific, I32450, 1:15-1:25) in 0.9% saline (Ricca, 7210-32) supplemental experimental procedures for 15 min on ice. A wholemount was placed on a chamber glass coverslip, dried with tissue paper, and attached by adding 100 μL of 100% matrigel without phenol red (Corning, 356231) in 1 mL of fusion medium (supplemental experimental procedures), incubating for 10 min at 37°C, 5% CO_2. The coverslip was placed in the POC-R2 perfusion chamber (Pecon) and infused with fusion medium using a 20 mL syringe with a 19-gauge needle. The chamber was placed on the Zeiss 780 stage. A peristaltic pump connected to gas-permeable tubes (Tygon Sanitary Silicone Tubing- ABW00002, 3350) circulated the fusion medium, which was incubated with 40% O_2 and 5% CO_2 throughout the recording period.

Time-lapse experiments were conducted on V-SVZ wholemounts from young (three 2-month-old and one 3-month-old) and aged (one 27-month-old and three 28-month-old) mice and one movie/V-SVZ/mouse. DMSO or ROCKi-treatment experiments used: young (four 2-month-old and three 3-month-old) mice and one movie/V-SVZ/mouse. Mice displaying signs of illness, severe dermatitis, or tumors were excluded from studies.

Time-lapse recording

Z-stack images (22 μm in depth) were taken every 9 min, each scan period was 3 min, over 20 h total, using a Zeiss 780 with a 40X water immersion objective. For ROCKi experiments, wholemounts were incubated for 2 h with vehicle (DMSO) or ROCKi (40 μM) in perfusion medium then imaged for at least 6 h following addition.

Video analysis and quantification

Imaris (9.7.0, Bitplane) was used to automatically calculate cell travel speed, distance traveled, track length and surface contact area and create 3D renderings. Cell ruffling and process counting were done manually after image processing in Imaris. For details of the image analysis, see supplemental experimental procedures.

Examining Rho GTPase signaling pathway gene changes with age

Gene expression data in V-SVZ subtypes from Table S2 in Kalamakis et al. (2019) were imported into RStudio. Genes for each cell subtype were filtered for statistical significance ($p < 0.05$) and then intersected with all genes within the GO category "cell migration" (GO: 0016477). Subsequent lists were analyzed for GO term

enrichment using the HypeR package (Federico and Monti, 2020) and the Reactome database. The background setting indicating the number of genes used for GO enrichment was 23,647.

The heatmap was generated by analyzing the number of genes expressed in selected pathways normalized to the number of genes within that pathway and was generated in R using the gplots package with colors from RColor Brewer.

Statistics

Statistical analyses were performed in GraphPad Prism 9. Description of the tests performed is provided in the figure legends.

Data and code availability

All code is available at https://www.neuralsci.org/computing.

SUPPLEMENTAL INFORMATION

Supplemental information can be found online at https://doi.org/10.1016/j.stemcr.2021.12.007.

AUTHOR CONTRIBUTIONS

S.T., K.Z., and X.Z. designed the experiments; X.Z., Y.W. and L.M. performed the time-lapse experiments and collected data; X.Z., K.Z., E.S.F., Y.W., and S.T. analyzed and interpreted data. All authors prepared figures and wrote, edited, and approved the manuscript.

CONFLICT OF INTERESTS

The authors declare no competing interests.

ACKNOWLEDGMENTS

This work was funded by National Institute on Aging (NIA) R01AG041861 (S.T.), National Institutes of Neurological Disorders and Stroke (NINDS) R35NS097277 (S.T.), and NINDS/NIA R01NS110749 (K.Z.). We thank Chris Bjornsson for contributions to time-lapse development and Joseph Mazurkiewicz at Albany Medical Center Imaging Core for Imaris software support. Schematics were created using Biorender.

Received: November 2, 2021
Revised: December 12, 2021
Accepted: December 13, 2021
Published: January 13, 2022

REFERENCES

Apostolopoulou, M., Kiehl, T.R., Winter, M., Cardenas De La Hoz, E., Boles, N.C., Bjornsson, C.S., Zuloaga, K.L., Goderie, S.K., Wang, Y., Cohen, A.R., et al. (2017). Non-monotonic changes in progenitor cell behavior and gene expression during aging of the adult V-SVZ neural stem cell niche. Stem Cell Rep. *9*, 1931–1947.

Borm, B., Requardt, R.P., Herzog, V., and Kirfel, G. (2005). Membrane ruffles in cell migration: indicators of inefficient lamellipodia adhesion and compartments of actin filament reorganization. Exp. Cell Res. *302*, 83–95.

Capilla-Gonzalez, V., Cebrian-Silla, A., Guerrero-Cazares, H., Garcia-Verdugo, J.M., and Quiñones-Hinojosa, A. (2014). Age-related changes in astrocytic and ependymal cells of the subventricular zone. Glia *62*, 790–803.

Codega, P., Silva-Vargas, V., Paul, A., Maldonado-Soto, A.R., Deleo, A.M., Pastrana, E., and Doetsch, F. (2014). Prospective identification and purification of quiescent adult neural stem cells from their in vivo niche. Neuron *82*, 545–559.

Cutler, R.R., and Kokovay, E. (2020). Rejuvenating subventricular zone neurogenesis in the aging brain. Curr. Opin. Pharmacol. *50*, 1–8.

De Marchis, S., Fasolo, A., Shipley, M., and Puche, A. (2001). Unique neuronal tracers show migration and differentiation of SVZ progenitors in organotypic slices. J. Neurobiol. *49*, 326–338.

Fernandez-Borja, M., Janssen, L., Verwoerd, D., Hordijk, P., and Neefjes, J. (2005). RhoB regulates endosome transport by promoting actin assembly on endosomal membranes through Dia1. J. Cell Sci. *118*, 2661–2670.

Federico, A., and Monti, S. (2020). hypeR: an R package for geneset enrichment workflows. Bioinformatics *36*, 1307–1308. https://doi.org/10.1093/bioinformatics/btz700.

Gage, F.H., and Temple, S. (2013). Neural stem cells: Generating and regenerating the brain. Neuron *80*, 588–601.

Guan, X., Guan, X., Dong, C., and Jiao, Z. (2020). Rho GTPases and related signaling complexes in cell migration and invasion. Exp. Cell Res. *388*, 111824.

James, R., Kim, Y., Hockberger, P.E., and Szele, F.G. (2011). Subventricular zone cell migration: Lessons from quantitative two-photon microscopy. Front. Neurosci. *5*, 30.

Kalamakis, G., Brüne, D., Ravichandran, S., Bolz, J., Fan, W., Ziebell, F., Stiehl, T., Catalá-Martinez, F., Kupke, J., Zhao, S., et al. (2019). Quiescence modulates stem cell maintenance and regenerative capacity in the aging brain. Cell *176*, 1407–1419.e1414.

Kim, E.J., Ables, J.L., Dickel, L.K., Eisch, A.J., and Johnson, J.E. (2011). Ascl1 (Mash1) defines cells with long-term neurogenic potential in subgranular and subventricular zones in adult mouse brain. PLoS One *6*, e18472.

Kim, Y., Comte, I., Szabo, G., Hockberger, P., and Szele, F.G. (2009). Adult mouse subventricular zone stem and progenitor cells are sessile and epidermal growth factor receptor negatively regulates neuroblast migration. PLoS One *4*, e8122.

Kokovay, E., Goderie, S., Wang, Y., Lotz, S., Lin, G., Sun, Y., Roysam, B., Shen, Q., and Temple, S. (2010). Adult SVZ lineage cells home to and leave the vascular niche via differential responses to SDF1/CXCR4 signaling. Cell Stem Cell *7*, 163–173.

Kurokawa, K., Itoh, R.E., Yoshizaki, H., Nakamura, Y.O., and Matsuda, M. (2004). Coactivation of Rac1 and Cdc42 at lamellipodia and membrane ruffles induced by epidermal growth factor. Mol. Biol. Cell. *15*, 1003–1010.

Law, A.K., Pencea, V., Buck, C.R., and Luskin, M.B. (1999). Neurogenesis and neuronal migration in the neonatal rat forebrain anterior subventricular zone do not require GFAP-positive astrocytes. Dev. Biol. *216*, 622–634.

Leong, S.Y., Faux, C.H., Turbic, A., Dixon, K.J., and Turnley, A.M. (2011). The Rho kinase pathway regulates mouse adult neural precursor cell migration. Stem Cells *29*, 332–343.

Luo, J., Daniels, S.B., Lennington, J.B., Notti, R.Q., and Conover, J.C. (2006). The aging neurogenic subventricular zone. Aging Cell *5*, 139–152.

Madisen, L., Zwingman, T.A., Sunkin, S.M., Oh, S.W., Zariwala, H.A., Gu, H., Ng, L.L., Palmiter, R.D., Hawrylycz, M.J., Jones, A.R., et al. (2010). A robust and high-throughput Cre reporting and characterization system for the whole mouse brain. Nat. Neurosci. *13*, 133–140.

Matta, R., Feng, Y., Sansing, L.H., and Gonzalez, A.L. (2021). Endothelial cell secreted VEGF-C enhances NSC VEGFR3 expression and promotes NSC survival. Stem Cell Res. *53*, 102318.

Mich, J.K., Signer, R.A., Nakada, D., Pineda, A., Burgess, R.J., Vue, T.Y., Johnson, J.E., and Morrison, S.J. (2014). Prospective identification of functionally distinct stem cells and neurosphere-initiating cells in adult mouse forebrain. Elife *3*, e02669.

Mirzadeh, Z., Merkle, F.T., Soriano-Navarro, M., Garcia-Verdugo, J.M., and Alvarez-Buylla, A. (2008). Neural stem cells confer unique pinwheel architecture to the ventricular surface in neurogenic regions of the adult brain. Cell Stem Cell *3*, 265–278.

Mishra, A.K., Campanale, J.P., Mondo, J.A., and Montell, D.J. (2019). Cell interactions in collective cell migration. Development *146*, dev172056.

Nam, S.C., Kim, Y., Dryanovski, D., Walker, A., Goings, G., Woolfrey, K., Kang, S.S., Chu, C., Chenn, A., Erdelyi, F., et al. (2007). Dynamic features of postnatal subventricular zone cell motility: A two-photon time-lapse study. J. Comp. Neurol. *505*, 190–208.

Obernier, K., Cebrian-Silla, A., Thomson, M., Parraguez, J.I., Anderson, R., Guinto, C., Rodas Rodriguez, J., Garcia-Verdugo, J.M., and Alvarez-Buylla, A. (2018). Adult neurogenesis is sustained by symmetric self-renewal and differentiation. Cell Stem Cell *22*, 221–234.e228.

Ota, H., Hikita, T., Sawada, M., Nishioka, T., Matsumoto, M., Komura, M., Ohno, A., Kamiya, Y., Miyamoto, T., Asai, N., et al. (2014). Speed control for neuronal migration in the postnatal brain by Gmip-mediated local inactivation of RhoA. Nat. Commun. *5*, 4532.

Pacary, E., Heng, J., Azzarelli, R., Riou, P., Castro, D., Lebel-Potter, M., Parras, C., Bell, D.M., Ridley, A.J., Parsons, M., et al. (2011). Proneural transcription factors regulate different steps of cortical neuron migration through Rnd-mediated inhibition of RhoA signaling. Neuron *69*, 1069–1084.

Pastrana, E., Cheng, L.C., and Doetsch, F. (2009). Simultaneous prospective purification of adult subventricular zone neural stem cells and their progeny. Proc. Natl. Acad. Sci. *106*, 6387–6392.

Ramirez-Castillejo, C., Sanchez-Sanchez, F., Andreu-Agullo, C., Ferron, S.R., Aroca-Aguilar, J.D., Sanchez, P., Mira, H., Escribano, J., and Farinas, I. (2006). Pigment epithelium-derived factor is a niche signal for neural stem cell renewal. Nat. Neurosci. *9*, 331–339.

Ridley, A.J. (2015). Rho GTPase signalling in cell migration. Curr. Opin. Cell Biol. *36*, 103–112.

Schaar, B.T., and McConnell, S.K. (2005). Cytoskeletal coordination during neuronal migration. Proc. Natl. Acad. Sci. U S A *102*, 13652–13657.

Shen, Q., Wang, Y., Kokovay, E., Lin, G., Chuang, S.M., Goderie, S.K., Roysam, B., and Temple, S. (2008). Adult SVZ stem cells lie in a vascular niche: A quantitative analysis of niche cell-cell interactions. Cell Stem Cell *3*, 289–300.

Shook, B.A., Manz, D.H., Peters, J.J., Kang, S., and Conover, J.C. (2012). Spatiotemporal changes to the subventricular zone stem cell pool through aging. J. Neurosci. *32*, 6947–6956.

Silva-Vargas, V., Crouch, E.E., and Doetsch, F. (2013). Adult neural stem cells and their niche: A dynamic duo during homeostasis, regeneration, and aging. Curr. Opin. Neurobiol. *23*, 935–942.

Tavazoie, M., Van der Veken, L., Silva-Vargas, V., Louissaint, M., Colonna, L., Zaidi, B., Garcia-Verdugo, J.M., and Doetsch, F. (2008). A specialized vascular niche for adult neural stem cells. Cell Stem Cell *3*, 279–288.

Vega, F.M., Fruhwirth, G., Ng, T., and Ridley, A.J. (2011). RhoA and RhoC have distinct roles in migration and invasion by acting through different targets. J. Cell Biol. *193*, 655–665.

Vega, F.M., and Ridley, A.J. (2018). The RhoB small GTPase in physiology and disease. Small GTPases *9*, 384–393.

Wherlock, M., Gampel, A., Futter, C., and Mellor, H. (2004). Farnesyltransferase inhibitors disrupt EGF receptor traffic through modulation of the RhoB GTPase. J. Cell Sci. *117*, 3221–3231.

Zhang, Z., Ottens, A.K., Larner, S.F., Kobeissy, F.H., Williams, M.L., Hayes, R.L., and Wang, K.K. (2006). Direct Rho-associated kinase inhibition [correction of inhibiton] induces cofilin dephosphorylation and neurite outgrowth in PC-12 cells. Cell. Mol. Biol. Lett. *11*, 12–29.

Zhao, X., Wang, Y., Wait, E., Mankowski, W., Bjornsson, C.S., Cohen, A.R., Zuloaga, K.L., and Temple, S. (2021). 3D image analysis of the complete ventricular-subventricular zone stem cell niche reveals significant vasculature changes and progenitor deficits in males versus females with aging. Stem Cell Rep. *16*, 836–850.

Zhu, C., Mahesula, S., Temple, S., and Kokovay, E. (2019). Heterogeneous expression of SDF1 retains actively proliferating neural progenitors in the capillary compartment of the niche. Stem Cell Rep. *12*, 6–13.

Zhuo, L., Sun, B., Zhang, C.-L., Fine, A., Chiu, S.-Y., and Messing, A. (1997). Live astrocytes visualized by green fluorescent protein in transgenic mice. Dev. Biol. *187*, 36–42.